

## Article

# Effective Combination of the Metal Centers in MOF-Based Materials toward Sustainable Oxidation Catalysts

Alexandre M. Viana <sup>1</sup>, Francisca Leonardes <sup>1</sup>, Marta C. Corvo <sup>2</sup>, Salette S. Balula <sup>1,\*</sup> and Luís Cunha-Silva <sup>1,\*</sup>

<sup>1</sup> LAQV-REQUIMTE, Department of Chemistry and Biochemistry, Faculty of Sciences, University of Porto, 4169-007 Porto, Portugal; up201405091@edu.fc.up.pt (A.M.V.); leonardes.francisca@gmail.com (F.L.)

<sup>2</sup> CENIMAT/I3N, Departamento de Ciência dos Materiais, Faculdade de Ciências e Tecnologia, Universidade Nova de Lisboa, 2829-516 Caparica, Portugal

\* Correspondence: sbalula@fc.up.pt (S.S.B.); l.cunha.silva@fc.up.pt (L.C.-S.)

**Abstract:** A successful encapsulation of Keggin-type polyoxomolybdate ( $H_3[PMo_{12}O_{40}]$ ,  $PMo_{12}$ ) into metal-organic framework (MOF) materials with an identical framework but distinct metal centers (ZIF-8 with  $Zn^{2+}$  and ZIF-67 with  $Co^{2+}$ ) was accomplished by a straightforward room-temperature procedure. The presence of  $Zn^{2+}$  in the composite material  $PMo_{12}@ZIF-8$  instead of  $Co^{2+}$  in  $PMo_{12}@ZIF-67$  caused a remarkable increase in the catalytic activity that achieved a total oxidative desulfurization of a multicomponent model diesel under moderate and friendly conditions (oxidant:  $H_2O_2$  and solvent: ionic liquid, IL). Interestingly, the parent ZIF-8-based composite with the Keggin-type polyoxotungstate ( $H_3[PW_{12}O_{40}]$ ,  $PW_{12}$ ),  $PW_{12}@ZIF-8$ , did not show the relevant catalytic activity. The ZIF-type supports present an appropriate framework to accommodate active polyoxometalates (POMs) into their cavities without leaching, but the nature of the metallic center from the POM and the metal present in the ZIF framework were vital for the catalytic performance of the composite materials.

**Keywords:** zeolitic imidazolate frameworks; polyoxometalates; nanocomposite material; oxidative desulfurization; heterogeneous catalysis



**Citation:** Viana, A.M.; Leonardes, F.; Corvo, M.C.; Balula, S.S.; Cunha-Silva, L. Effective Combination of the Metal Centers in MOF-Based Materials toward Sustainable Oxidation Catalysts. *Materials* **2023**, *16*, 3133. <https://doi.org/10.3390/ma16083133>

Academic Editor: Cai Shen

Received: 27 March 2023

Revised: 6 April 2023

Accepted: 10 April 2023

Published: 16 April 2023



**Copyright:** © 2023 by the authors. Licensee MDPI, Basel, Switzerland. This article is an open access article distributed under the terms and conditions of the Creative Commons Attribution (CC BY) license (<https://creativecommons.org/licenses/by/4.0/>).

## 1. Introduction

Fossil fuels continue to be the major energy source that is applied for several purposes on which we are reliant, such as transportation; thus, much attention is now being focused on fossil fuel consumption as well as its production and processing, answering the calls for the ever-growing need for sustainable development [1]. One of the most relevant problems associated with the combustion of oil fuels is the emission of sulfur-derived products to the atmosphere, such as various sulfur oxides and particulate metal sulfates, which stem from the different sulfur-containing compounds (SCCs) that make up part of the original composition of crude oil, including thiophenes, sulfides and disulfides, mercaptans, dibenzothiophenes, and many other derived species [2]. If these SCCs are not discarded from the fuel matrix before combustion, their emissions will cause some environmental issues that are linked to acid rain and associated with several public health problems [3]. To mitigate these serious problems, the petrochemical industry must abide by international legislative regulation concerning the sulfur content that is present in processed fossil fuels, resorting to desulfurization processes [4]. The presence of these compounds is also undesirable during some stages of the refining process, as they can promote equipment corrosion and deactivation of the catalysts. Hydrodesulfurization (HDS) is the main approach that is currently used to remove SCCs from fuels in industrial plants, as it manages to efficiently convert the sulfur content to hydrogen sulfide and sulfur-free organic compounds [5]. HDS is dependent on high temperatures and pressures for hydrogen-consuming catalytic processes, which, knowing its lower efficiency to eliminate

heterocyclic compounds such as thiophenes, makes it an undesirably costly method to produce sulfur-free fuels [6].

Oxidative desulfurization (ODS) is an emerging and potentially cost-effective approach to desulfurize fuel derivatives, since it can accomplish the efficient removal of the most refractory thiophenes and dibenzothiophenes under sustainable conditions, i.e., low pressure and temperature, and avoid the consumption of hydrogen [7]. The ODS process is performed in two main steps: initially, the oxidation of SCCs to their corresponding sulfones or sulfoxides occurs, in which an oxidizing agent is needed for the contribution of one or two oxygen atoms, respectively; after, the extraction occurs, for which a suitable extracting solvent needs to be selected. Naturally, the first stage is enabled by catalytic systems, for which an adequate catalyst must be appointed, and many different types of materials can be considered for this task; polyoxometalates (POMs) are credited as one of the most interesting ones [8].

POMs are polyatomic ions based on transition metal oxyanions that are recognized for their structural diversity, interesting chemical properties, and potential applicability in several areas. These are assembled by  $\text{MO}_x$  coordination polyhedra (M: transition metal; x: 4, 5 or 6), which can result in various topological motifs [9]. Keggin arrangements are well-known POM structures that share a  $[\text{X}^{n+}\text{M}_{12}\text{O}_{40}]^{(8-n)-}$  (X stands for a heteroatom from block p or d) formula that is built around a central  $\text{XO}_4$  tetrahedron that is enclosed in twelve  $\text{MO}_6$  octahedrons and organized in groups of  $\text{M}_3\text{O}_{13}$  units that are linked by O vertex atoms to form a spherical structure with tetrahedral symmetry. Usually, POMs are effective catalysts in a vast number of distinct reactions, and the Keggin POMs have revealed themselves to be particularly useful as selective catalysts of oxidation reactions, where ODS reactions can be included [10,11]. Still, these can be associated with the usual drawbacks that are related to homogeneous catalysts, namely, poor recyclability potential, which is a very important parameter to consider when looking for an efficient oxidative desulfurization catalytic system as an alternative for the HDS process. Many strategies have been proposed to solve this problem, such as their heterogenization by encapsulation in suitable support materials, such as porous metal–organic frameworks (MOFs) [12]. This new family of materials includes coordination polymers formed by metal cations or clusters interconnected by organic linkers (ligands) originating from crystalline and microporous coordination frameworks. MOFs are very popular due to their structural diversity and their simply tunable properties, giving them enormous potential for a wide range of applications, such as gas separation and/or storage, chemical sensors, heterogeneous catalysts, platforms for drug delivery, and energy storage [13–17].

Following our research endeavors on functional crystalline materials and the oxidative desulfurization process [18–24], also including zeolitic imidazolate framework (ZIF) materials [25,26], an innovative study that compares the catalytic efficiency of different combinations of polyoxometalates encapsulated in ZIF supports with distinct metallic centers is reported. ZIFs are a well-known subclass of crystalline and porous MOFs that have frameworks analogous to those found in zeolites. The encapsulation of active Keggin POMs as  $\text{H}_3[\text{PMo}_{12}\text{O}_{40}]$  ( $\text{PMo}_{12}$ ) and  $\text{H}_3[\text{PW}_{12}\text{O}_{40}]$  ( $\text{PW}_{12}$ ) was performed in situ with MOF assembling (Figure 1). ZIF-8 and ZIF-67 are highly stable isostructural  $\text{M}(\text{2-mim})_2$  frameworks (M: respectively  $\text{Zn}^{2+}$  and  $\text{Co}^{2+}$ ; 2-mim: 2-methylimidazole) with sodalite-type topology and cavities built upon  $\text{MN}_4$  tetrahedral units [27]. The key reason for the selection of these two structures as hosts for guest POMs was the match between their dimension (10 Å) and the MOFs pore size (11.6 Å), which was related to the smaller pore window (3.4 Å) and could prevent leaching [28]. Therefore, probably only one POM unit can fit into a cage of ZIF materials. The small pore window will guarantee the absence of POM leaching but can simultaneously hinder the diffusion of the reactants to meet the active center that is entrapped in the ZIF cage. This is probably the reason for the scarce amount of work reported in the literature that uses ZIF materials as heterogeneous catalysts in the liquid phase [25,26,29,30].

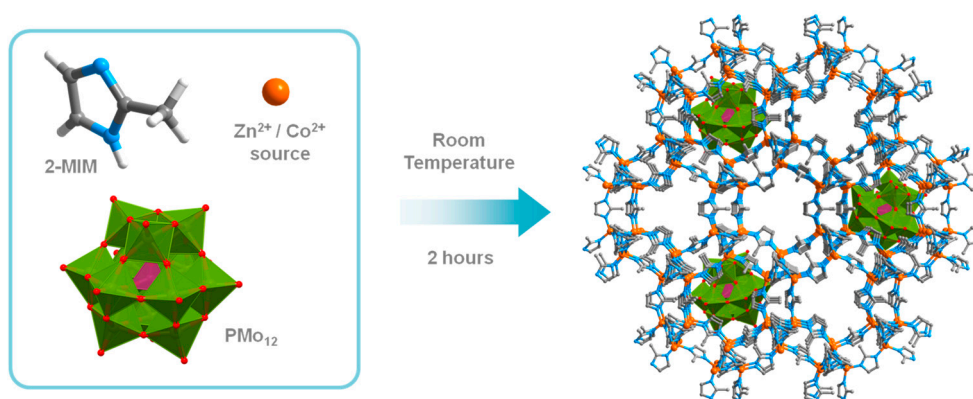


**Figure 1.** Schematic representation of the in situ sustainable preparation of the PMo<sub>12</sub>@ZIF composite materials.

## 2. Experimental Section

### 2.1. Materials and Characterization Methods

Phosphomolybdic acid (H<sub>3</sub>PMo<sub>12</sub>O<sub>40</sub>·xH<sub>2</sub>O, PMo<sub>12</sub>, microscopy grade; Sigma-Aldrich, Waltham, MA, USA), acid phosphotungstic (H<sub>3</sub>PW<sub>12</sub>O<sub>40</sub>·xH<sub>2</sub>O, PW<sub>12</sub>, microscopy grade, Sigma-Aldrich), cobalt(II) nitrate (Co(NO<sub>3</sub>)<sub>2</sub>·6H<sub>2</sub>O, > 99.8%, Sigma-Aldrich), Zinc(II) nitrate (Zn(NO<sub>3</sub>)<sub>2</sub>·4H<sub>2</sub>O > 98.5%, Merck, Rahway, NJ, USA), 2-methylimidazole (C<sub>4</sub>H<sub>6</sub>N<sub>2</sub>, 99.0%, 2-mIm, Sigma-Aldrich), 1-butyl-3-methylimidazole hexafluorophosphate (C<sub>8</sub>H<sub>15</sub>F<sub>6</sub>N<sub>2</sub>P > 97%, bmImPF<sub>6</sub>, Sigma-Aldrich), tetradecane (C<sub>14</sub>H<sub>30</sub> > 99.0%, Sigma-Aldrich), hydrogen peroxide (H<sub>2</sub>O<sub>2</sub>, aqueous 30%, Sigma-Aldrich), *N,N*-dimethylformamide (C<sub>3</sub>H<sub>7</sub>NO, DMF, 99.99%, Fisher, Waltham, MA, USA), ethanol (C<sub>2</sub>H<sub>5</sub>OH, EtOH > 99.8%, Fisher), methanol (CH<sub>3</sub>OH, MeOH, analytical reagent grade, Fisher), acetonitrile (CH<sub>3</sub>CN, MeCN > 99.5%, Fluka, Buchs, Switzerland), benzothiophene (C<sub>8</sub>H<sub>6</sub>S, BT, > 95%, Fluka), *N*-octane (C<sub>8</sub>H<sub>18</sub> > 99.0%, Acros Organic, Geel, Belgium), dibenzothiophene (C<sub>12</sub>H<sub>8</sub>S, 98%, DBT, Sigma-Aldrich), and 4-methyldibenzothiophene (C<sub>13</sub>H<sub>10</sub>S, MDBT, 96%, Sigma-Aldrich) 4,6-dimethyldibenzothiophene (C<sub>14</sub>H<sub>12</sub>S, DMDBT, 95%, Acros Organic) were acquired from commercial sources and used as received.

Fourier-transformed infrared (FTIR) spectra were acquired in the attenuated total reflectance (ATR) operation mode of a PerkinElmer (Waltham, MA, USA) FTIR System Spectrum BX spectrometer, and all the representations are shown in arbitrary units of transmittance. Powder X-ray diffraction (XRD) patterns were obtained at room temperature on a Rigaku (Tokyo, Japan) Geigerflex diffractometer operating with a Cu radiation source ( $\lambda_1 = 1.540598 \text{ \AA}$ ;  $\lambda_2 = 1.544426 \text{ \AA}$ ;  $\lambda_1/\lambda_2 = 0.500$ ) and in a Bragg–Brentano  $\theta/2\theta$  configuration (45 kV, 40 mA). Intensity data were collected by a step-counting method (step 0.026°) in continuous mode in the  $3 \leq 2\theta \leq 50^\circ$  range, and all the representations are shown in arbitrary units of intensity. Scanning electron microscopy (SEM) and electron dispersive X-ray spectroscopy (EDS) analysis were performed in a FEI (Lausanne, Switzerland) Quanta 400 FEG ESEM high-resolution scanning electron microscope equipped with an EDAX Genesis X4M spectrometer working at 15 kV. Samples were coated with an Au/Pd thin film by sputtering using a SPI Module Sputter Coater equipment. Solid state <sup>31</sup>P nuclear magnetic resonance (NMR) spectra were acquired with an 11 T (500 MHz) AVANCE II+ Bruker spectrometer operating at 202.45 MHz, equipped with a BBO probe head. The samples were spun at the magic angle (MAS) at a frequency of 5 kHz in 4 mm-diameter rotors at room temperature and the spectra were obtained with proton cross-polarization (CPMAS) with a contact time of 5.0 ms and the recycle delay was 5.0 s. Inductively coupled plasma optical emission spectroscopy (ICP-OES) was used to quantify Mo concentrations in various samples, resorting to a PerkinElmer Otima 4300 DV. N<sub>2</sub> adsorption–desorption isotherms were collected at −196 °C with a gas porosimeter Micromeritics ASAP 2010. Pre-outgassing of the analyzed samples was carried out at 150 °C for 2 h. Catalytic reactions were periodically monitored by GC-FID analysis carried out in a Bruker 430-GC-FID

chromatograph. Hydrogen was used as carrier gas ( $55 \text{ cm}\cdot\text{s}^{-1}$ ) and fused silica Supelco (St. Louis, MO, USA) capillary columns SPB-5 ( $30 \text{ m} \times 0.25 \text{ mm i. d.}$ ;  $25 \text{ }\mu\text{m}$  film thickness) were used.

## 2.2. Materials Preparation

### Supports ZIF-8 and ZIF-67

The support materials were prepared by an adaptation of the experimental procedure previously reported [28]. Briefly, primary solutions of  $\text{Zn}(\text{NO}_3)_2\cdot 4\text{H}_2\text{O}$  or  $\text{Co}(\text{NO}_3)_2\cdot 6\text{H}_2\text{O}$  (2.5 mmol) in MeOH (25 mL) were stirred magnetically for 15 min to prepare the Zn-based MOF (ZIF-8) and Co-based MOF (ZIF-67), respectively. After, solutions of 2-mIm (19.8 mmol) in MeOH (25 mL) were prepared and slowly added to the respective metal-containing solutions. The Zn- and Co-based resulting reactional mixtures were stirred (magnetically) for 150 min, at room temperature and ambient pressure. Lastly, the obtained solid materials were isolated by centrifugation, washed with MeOH (five times), and dried under vacuum at  $60 \text{ }^\circ\text{C}$  for 12 h.

### $\text{PMo}_{12}$ @ZIF-8

This procedure is adaptation of the previously mentioned methods using a one-pot procedure for the preparation of POM composites. An aqueous solution (10 mL) of  $\text{PMo}_{12}$  (125 mg) was joined to the primary  $\text{Zn}^{2+}$  solution: 2.5 mmol of  $\text{Zn}(\text{NO}_3)_2\cdot 4\text{H}_2\text{O}$  in 25 mL of MeOH. This resulting mixture was stirred (magnetically) for 30 min, after which 2-mIm methanolic solution (19.8 mmol in 25 mL of MeOH) was likewise added. The resulting reactional mixtures were stirred (magnetically) for 150 min at room temperature and ambient pressure. Lastly, the obtained solid materials were isolated by centrifugation, washed with MeOH (five times), and dried at under vacuum at  $60 \text{ }^\circ\text{C}$  for 12 h. Atomic ratio of Zn/Mo = 1.86.

### $\text{PW}_{12}$ @ZIF-8

An aqueous solution (10 mL) of  $\text{PW}_{12}$  (125 mg) was joined to a  $\text{Zn}^{2+}$  solution: 2.5 mmol of  $\text{Zn}(\text{NO}_3)_2\cdot 4\text{H}_2\text{O}$  in 25 mL of MeOH. This resulting mixture was stirred (magnetically) for 30 min, after which 2-mIm methanolic solution (19.8 mmol in 25 mL of MeOH) was likewise added. The resulting reactional mixtures were stirred (magnetically) for 150 min at room temperature and ambient pressure. Lastly, the obtained solid materials were isolated by centrifugation, washed with MeOH (five times), and dried at under vacuum at  $60 \text{ }^\circ\text{C}$  for 12 h. Atomic ratio of Zn/W = 1.41.

### $\text{PMo}_{12}$ @ZIF-67

An aqueous solution (10 mL) of  $\text{PMo}_{12}$  (125 mg) was joined to the initial  $\text{Co}^{2+}$  solution: 2.5 mmol of  $\text{Co}(\text{NO}_3)_2\cdot 6\text{H}_2\text{O}$  in 25 mL of MeOH. This resulting mixture was stirred for 30 min, after which 2-mIm methanolic solution (19.8 mmol in 25 mL of MeOH) was added. The resulting reactional mixtures were stirred for 150 min at room temperature and ambient pressure. Lastly, the obtained solid materials were isolated by centrifugation, washed with MeOH (five times), and dried at under vacuum at  $60 \text{ }^\circ\text{C}$  for 12 h. Atomic ratio of Co/Mo = 0.67.

## 2.3. Oxidative Desulfurization Studies

The prepared ZIF supports and the POM@ZIF composites were evaluated as heterogeneous catalysts for ODS systems in a multicomponent model diesel comprising the SCCs, BT (500 ppm od S), DBT (500 ppm of S), MDBT (500 ppm of S), and DMDBT (500 ppm of S) in *n*-octane. The reactions were performed in a closed vessel, under air in a closed borosilicate vessel with a magnetic stirrer and immersed in a thermostatically controlled liquid paraffin bath at  $70 \text{ }^\circ\text{C}$ . Oxidative catalytic desulfurization experiments were performed in a biphasic system composed by the model diesel and [BMIM]PF<sub>6</sub> as extraction solvent. In a representative experiment, a certain amount of the catalyst material containing an equivalent of 3 mmol of active center POM was added to 0.75 mL of [BMIM]PF<sub>6</sub> and 0.75 mL of model diesel, and this mixture was stirred for 10 min at  $70 \text{ }^\circ\text{C}$ . The oxidative catalytic step was initiated with the addition of aqueous H<sub>2</sub>O<sub>2</sub> 30% (75  $\mu\text{L}$ ) to system.

Tetradecane was used as a standard in the periodical monitorization of the sulfur content by GC analysis. At the end of each reaction, catalysts were recovered by centrifugation, washed carefully, and for three times with MeCN and EtOH, they were dried at 60 °C overnight under vacuum and reused in the subsequent catalytic cycle, which had identical reaction conditions. The desulfurization was quantified by analyzing the model diesel phase, which was withdrawn from upper phase (20  $\mu$ L) and analyzed with addition of tetradecane as standard by gas chromatography to quantify the total sulfur content. Finally, the desulfurization efficiency (%) was calculated according to the following formula: Desulfurization efficiency (%) = (initial sulfur content-residual sulfur content)/(initial sulfur content)  $\times$  100 %.

### 3. Results and Discussion

#### 3.1. Materials Characterization

The supporting materials ZIF-8 and ZIF-67 and the composites PMo<sub>12</sub>@ZIF-8, PW<sub>12</sub>@ZIF-8, and PMo<sub>12</sub>@ZIF-67 were prepared through a straightforward room-temperature experimental procedure based on the previously reported synthesis methods [31,32]. All the isolated materials were characterized by powder XRD, FTIR spectroscopy, SEM/EDS, and N<sub>2</sub> adsorption-desorption isotherms. The vibrational spectra of the materials depict that the main absorption bands are predictable from the MOF structures (Figure 2a): a very strong band observed around 420 cm<sup>-1</sup> assigned to metal-nitrogen coordination, strong and weak bands from 600 up to 1500 cm<sup>-1</sup> can be attributed to C–N ring bonds, and a weak vibration band seen at 1580 cm<sup>-1</sup> is assigned to the C=N bond [33,34]. Additionally, in the composite materials (PMo<sub>12</sub>@ZIF-8, PW<sub>12</sub>@ZIF-8, and PMo<sub>12</sub>@ZIF-67) spectra, a group of medium intensity bands are evident in the interval from 770 to 975 cm<sup>-1</sup>. These absorption bands can be assigned to Mo=O and Mo–O, or W=O and W–O, bond vibration bands from PMo<sub>12</sub> or PW<sub>12</sub> incorporated in the ZIFs vacancies, respectively [35]. Weak protuberances between 1000 and 1100 cm<sup>-1</sup> can be associated with P–O bond vibrations and further support these results.

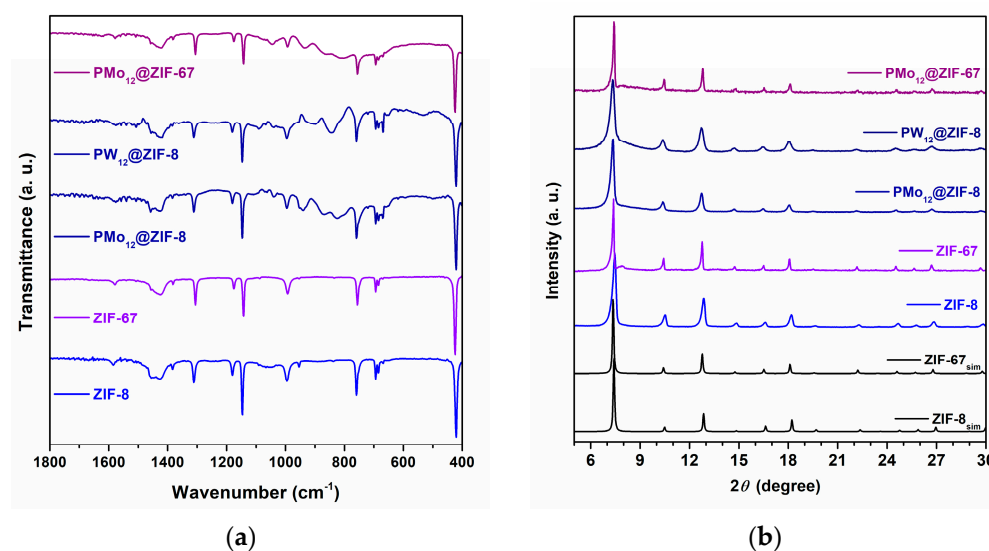


**Figure 2.** FTIR spectra (a) and Powder XRD patterns (b) obtained for ZIF-8, ZIF-67, and POM@ZIF composite materials (PMo<sub>12</sub>@ZIF-8, PW<sub>12</sub>@ZIF-8, and PMo<sub>12</sub>@ZIF-67).

The powder XRD patterns registered for the pristine MOF samples ZIF-8 and ZIF-67 (Figure 2b) are consonant with the previously reported diffraction patterns for these crystalline structures, revealing the expected characteristic peaks with the correct relative intensities [36]. Furthermore, the PMo<sub>12</sub>@ZIF-8, PW<sub>12</sub>@ZIF-8, and PMo<sub>12</sub>@ZIF-67 samples revealed comparable unique-phase diffraction patterns, suggesting the effective formation of ZIF structures as composite frameworks. The absence of characteristic reflections of

the POMs points to the random distribution of POMs in the framework of the ZIFs, most probably as a consequence of an effective and nonregular impregnation of the POMs in the cavities of the ZIFs.

SEM micrographs obtained for ZIF-8 and ZIF-67 samples reveal an aggregation of uniform particles with a rhombic dodecahedron morphology and regular sizes distributed around 100 nm and between 600 and 800 nm, respectively (Figure 3). Interestingly, the  $\text{PMo}_{12}$ @ZIF-8 micrograph shows particles with an identical size but with a lower degree of morphological uniformity (Figure 3 above, right). In these, the regular distribution of Mo and P revealed by the EDS analysis suggests a uniform distribution of the  $\text{PMo}_{12}$  on ZIF-8. Particles with an irregular size distribution are evidenced for  $\text{PMo}_{12}$ @ZIF-67 (Figure 3 below, right). The EDS spectrum recorded for this sample shows Mo and P peaks, although distributed in an irregular fashion through the sample, as smaller particles that are associated with a higher Mo content (Figure 3 below, right).

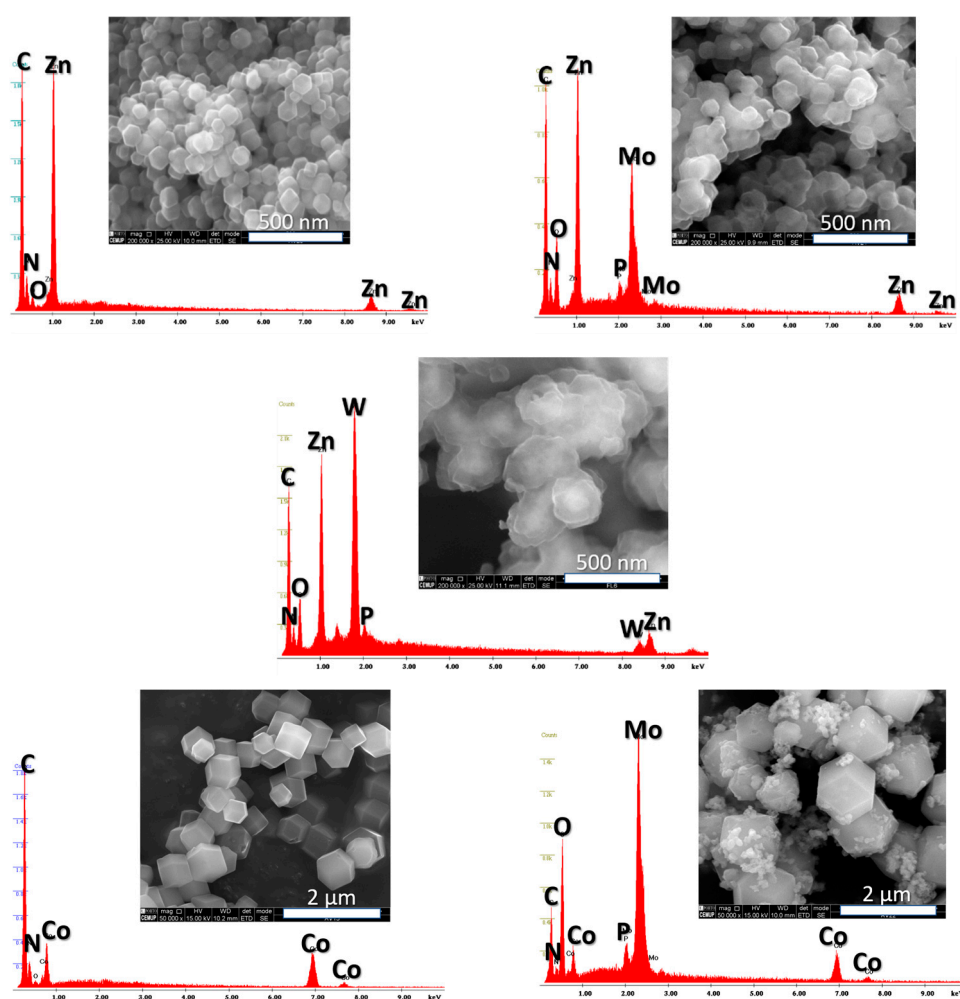


**Figure 3.** SEM micrographs and corresponding EDS spectra recorded for ZIF-8 (above, left),  $\text{PMo}_{12}$ @ZIF-8 (above, right),  $\text{PW}_{12}$ @ZIF-8 (middle), ZIF-67 (below, left), and  $\text{PMo}_{12}$ @ZIF-67 (below, right).

$\text{N}_2$  sorption isotherms of both MOFs and derived POM@MOF composite materials were acquired (Figure 4), and the estimated BET parameters are systematized in Table 1. All analyzed samples show type-I isotherms that are related to their expected microporosity. The specific surface areas calculated for ZIF-8 and ZIF-67 are in accordance with previously reported values for these structures [31,37]. An introduction of the POM units inside the MOFs cavities should result in a lower available surface area for  $\text{N}_2$  absorption.

The consistently lower surface areas calculated for POM@MOFs are evidence of the successful preparation of these materials.  $\text{PMo}_{12}$ @ZIF-8 and  $\text{PW}_{12}$ @ZIF-8 were studied by ICP-OES to determine Mo or W concentrations and quantify  $\text{PMo}_{12}$  (0.15 mmol/g) or  $\text{PW}_{12}$  (1.6 mmol/g) inserted in the cavities of MOFs, in order to calculate the catalyst quantities that correspond to 3  $\mu\text{mol}$  of an active POM to be used in ODS.

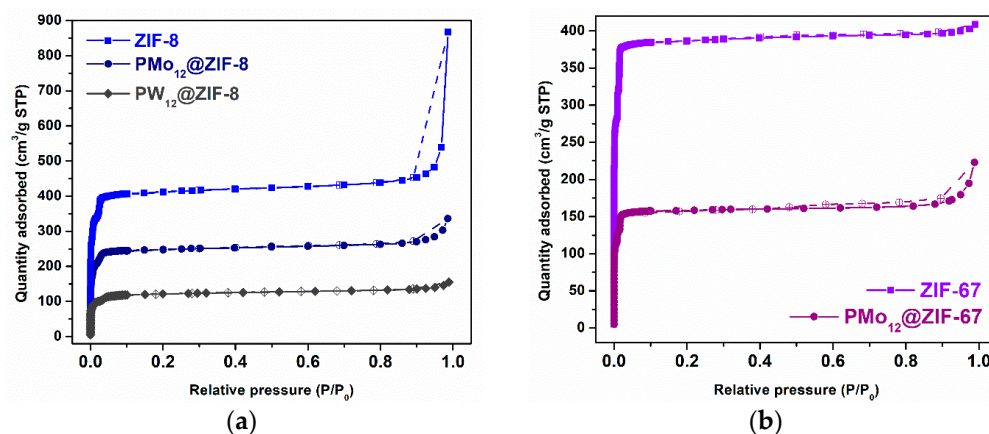


**Figure 4.**  $\text{N}_2$  adsorption–desorption isotherms at  $-196\text{ }^\circ\text{C}$  of both MOFs and POM@MOF composite materials: (a) ZIF-8 and ZIF-8 based materials; (b) ZIF-67 and ZIF-67 based materials. Filled and unfilled symbols relate to adsorption and desorption processes, respectively.

**Table 1.** BET optimized parameters calculated for of both ZIF structures and POM@ZIF composite materials.

Sample	$S_{\text{BET}}$ ( $\text{m}^2/\text{g}$ )	$V_{\text{P}}$ ( $\text{cm}^3/\text{g}$ )
ZIF-8	1743	0.61
ZIF-67	1712	0.58
$\text{PMo}_{12}$ @ZIF-8	1044	0.37
$\text{PW}_{12}$ @ZIF-8	490	0.18
$\text{PMo}_{12}$ @ZIF-67	711	0.24

( $S_{\text{BET}}$ ): BET specific surface area; ( $V_{\text{P}}$ ): total pore volume determined at  $P/P_0 = 0.99$ .

### 3.2. Catalytic Desulfurization Studies

Oxidative desulfurization studies were carried out at  $70\text{ }^\circ\text{C}$  in a biphasic system based on equal volumes of the model diesel and extraction solvent. The ionic liquid 1-butyl-3-methylimidazole hexafluorophosphate ( $[\text{BMIM}]\text{PF}_6$ ) was utilized as an extraction solvent and the oxidizing agent used was the aqueous hydrogen peroxide. The model diesel was prepared with various SCCs representative of the most refractory sulfur content present in diesel fuels, namely BT, DBT, MDBT, and DMDBT. Initially, an extractive desulfurization occurred every 10 min by mixing both liquid phases (1:1)  $[\text{BMIM}]\text{PF}_6$ /model diesel. After this, the equilibrium of sulfur components extracted from diesel in the ionic liquid phase was reached, and to increase the desulfurization efficiency, the oxidant  $\text{H}_2\text{O}_2$  is added to the system to cause the oxidative desulfurization. When the sulfur components that are present in the extraction phase are oxidized to sulfones and/or sulfoxides, more sulfur compounds are extracted from the diesel phase (ECODS, extraction, and catalytic oxidative desulfurization system).

Preliminary ECODS tests were performed using the homogeneous catalytic active centers  $\text{PMo}_{12}$  and  $\text{PW}_{12}$ , and also the support materials ZIF-8 and ZIF-67, to assess their inherent catalytic behavior (Figure 5a).  $\text{PMo}_{12}$  and  $\text{PW}_{12}$  promoted near total desulfurization of the model diesel (99.8%) after 1 h of reaction time, while both ZIF-8 and ZIF-67 did not exhibit any catalytic activity toward ODS. Further, the composite materials  $\text{PMo}_{12}$ @ZIF-8,  $\text{PMo}_{12}$ @ZIF-67, and  $\text{PW}_{12}$ @ZIF-8 were evaluated as heterogeneous catalysts for ECODS

processes (Figure 5b), with the POMs as the active center since the ZIF supports did not show any catalytic activity. As the parent MOF,  $\text{PMo}_{12}$ @ZIF-67 does not show any catalytic activity, which suggests that the active  $\text{PMo}_{12}$  incorporated in the ZIF-67 framework cannot achieve its role as a catalyst. On the other hand,  $\text{PMo}_{12}$ @ZIF-8 displays heterogeneous catalytic behavior toward ECODS, as it promotes high desulfurization of the model diesel (90.7%) after 2 h. At the end of this first catalytic cycle, the material was recovered, washed repeatedly, and dried. After this, the  $\text{PMo}_{12}$ @ZIF-8 was used in nine consecutive ECODS cycles for 2 h. The guaranteed, consistent catalytic results confirm a great recycling potential (Figure 5b). Additionally, comparing the catalytic performances of  $\text{PW}_{12}$  and  $\text{PMo}_{12}$  incorporated into the ZIF-8 framework, it is possible to observe that the composite  $\text{PW}_{12}$ @ZIF-8 presents much lower oxidative desulfurization efficiency, since the desulfurization only increased by 20% after the initial extraction step, instead of the 50% increase obtained using the  $\text{PMo}_{12}$ @ZIF-8 catalyst. This low activity of  $\text{PW}_{12}$ @ZIF-8 must be due to the low accessibility of the  $\text{PW}_{12}$  active center for interaction with sulfur compounds and oxidants, which is probably caused by its higher POM loading (approximately ten times more) than the  $\text{PMo}_{12}$ @ZIF-8 composite. On the other hand, the  $\text{PMo}_{12}$ @ZIF-67 composite presents a  $\text{PMo}_{12}$  loading that is only slightly higher than the  $\text{PMo}_{12}$ @ZIF-8 composite; however, an absence of oxidative catalytic activity was found when using the ZIF-67 composite.

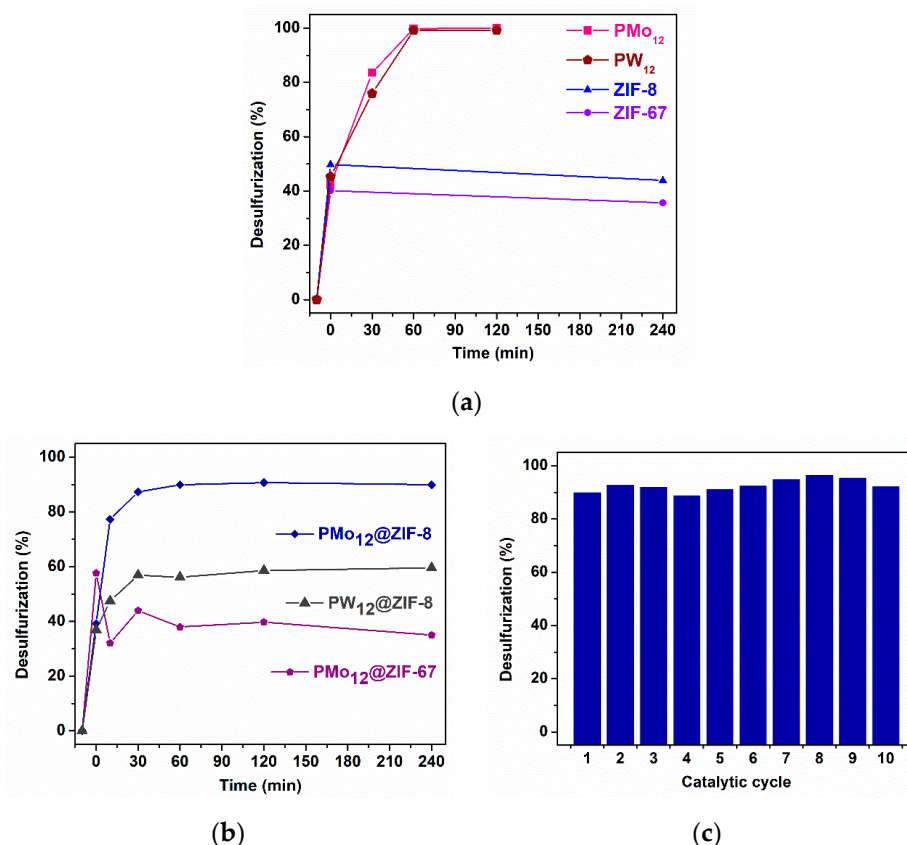


**Figure 5.** (a) Catalytic behavior of homogeneous POMs,  $\text{PMo}_{12}$  and  $\text{PW}_{12}$ , and supporting MOFs, ZIF-8 and ZIF-67. Assays were performed at 70 °C in a model fuel/[BMIM]PF<sub>6</sub> biphasic system with 3  $\mu\text{mol}$  of POM or 15 mg of MOF. ODS reaction starts at 0 min with the addition of aq.  $\text{H}_2\text{O}_2$ , after a 10 min extraction step. (b) Desulfurization profile of a multicomponent model fuel using  $\text{PMo}_{12}$ @ZIF-8,  $\text{PW}_{12}$ @ZIF-8, and  $\text{PMo}_{12}$ @ZIF-67 catalysts, [BMIM]PF<sub>6</sub> extraction solvent,  $\text{H}_2\text{O}_2$  oxidant, at 70 °C. (c) Recycling desulfurization process for ten consecutive cycles (2 h each reaction) using  $\text{PMo}_{12}$ @ZIF-8 catalyst.

A comparative study was performed between the active  $\text{PMo}_{12}$ @ZIF-8 and the other reported  $\text{PMo}_{12}$ -based MOF catalysts used for the oxidative desulfurization of refractory

model fuels. The results are summarized in Table 2. It is possible to observe that the active  $\text{PMo}_{12}$  active center was immobilized in several MOF structures, including UiO-66, UiO-67, and ZIF-6; however, most of these  $\text{PMo}_{12}$ @MOFs catalysts were tested in single model fuels mainly containing the refractory sulfur compounds that are the easiest to oxidize and remove from model and real fuels, the DBT [38–43]. An identical multicomponent model diesel was used by Granadeiro et al. by incorporating  $\text{PMo}_{12}$  into porous  $\text{NH}_2$ -MIL-101(Cr) [21]. Using this composite, near-complete desulfurization was achieved after 2 h; however, the recycling capacity was only verified up to three consecutive cycles. Last year, Zhou et al. used the  $\text{PMo}_{12}$ @MOF-199 catalyst to desulfurize a 4,6-DMDBT single model fuel under aerobic reaction conditions [44]. Using molecular oxygen as an oxidant, a higher reaction temperature of 120 °C was needed to achieve 90% desulfurization after a short reaction time [44]. This was a successful result since 4,6-DMDBT is one of the most stubborn sulfides in fuel oil. Further, the  $\text{PMo}_{12}$ @MOF-199 catalyst showed itself to be recyclable and stable under aerobic conditions. Yang et al. presented a porous ionic liquid catalyst using ZIF-8 support [42]. The intention to use the PIL functional group promoted the contact between the oxidant  $\text{H}_2\text{O}_2$  and the active center  $\text{PMo}_{12}$ . However, only single model DBT fuel was used, and even if complete desulfurization was achieved, a longer period of time (2 h) was needed without information concerning the stability and recycling capacity of this catalyst [42]. In 2021, Fernandes et al. used a model diesel containing three different sulfur compounds (1-BT, DBT, and 4-MDBT) that were completely desulfurized after 1 h of using the  $\text{PMo}_{12}$ @MOF-808 catalyst. Stability and recycle capacity were confirmed [45]. This last composite is a promising one with a high efficiency and stability; however, its activity to desulfurize the hardest sulfur compound to be oxidized and extracted (4,6-DMDBT) is unknown.

**Table 2.** Comparison of catalytic efficiency of reported  $\text{PMo}_{12}$ @MOFs composites for desulfurization of model fuels.

Catalyst	Sulfur	Temperature (°C)	Time (h)	Oxidant	Efficiency (%)	Reference
$\text{PMo}_{12}$ @ $\text{NH}_2$ -MIL-101	1-BT, DBT, 4-MDBT, and 4,6-DMDBT	50	3	$\text{H}_2\text{O}_2$	95	[44]
$\text{PMo}_{12}$ @UiO-66 <sup>c</sup>	DBT	60	1	TBHP	100	[38]
$\text{PMo}_{12}$ @UiO-66	DBT	60	1	$\text{H}_2\text{O}_2$	100	[39]
$\text{PMo}_{12}$ @MOF-199	4,6-DMDBT	120	1.5	$\text{O}_2$	90	[44]
$\text{PMo}_{12}$ @UiO-67	T <sup>d</sup> and DBT	60	0.5	$\text{H}_2\text{O}_2$	100	[11]
$\text{PMo}_{12}$ @ZIF-67	DBT	70	3	TBHP	98	[40]
$\text{PMo}_{12}$ @MOF-808	1-BT, DBT, and 4-MDBT	70	1	$\text{H}_2\text{O}_2$	100	[45]
$\text{PMo}_{12}$ @MOF-808	DBT	50	1.5	$\text{H}_2\text{O}_2$	100	[41]
$\text{PMo}_{12}$ @ZIF-8-PIL <sup>a</sup>	DBT	r.t. <sup>b</sup>	2	$\text{H}_2\text{O}_2$	100	[42]
$\text{PMo}_{12}$ @DUT-67	DBT	50	1.5	$\text{H}_2\text{O}_2$	98	[43]
$\text{PMo}_{12}$ @ZIF-8	1-BT, DBT, 4-MDBT, and 4,6-DMDBT	70	2	$\text{H}_2\text{O}_2$	91	This work

<sup>a</sup> PIL: porous ionic liquids. <sup>b</sup> r.t.: room temperature. <sup>c</sup> calcinated composite. <sup>d</sup> T: thiophene.

The pristine support and the composite materials were recovered, washed, and dried after catalytic experiments (AC), and characterized to assess the distinguishing structural features after catalytic use. The powder XRD patterns obtained for ZIF-67(AC) and  $\text{PMo}_{12}$ @ZIF-67(AC) (Figure 6a) correspond to the original diffractograms and show structural maintenance for both samples. The same is found for ZIF-8(AC) and for  $\text{PW}_{12}$ @ZIF-8(AC) (Figure 6b): even though the registered relative peak intensity slightly varies, the crystalline structure of ZIF-8 seems stable under catalytic conditions. Active  $\text{PMo}_{12}$ @ZIF-8 apparently undergoes structural transformations that are manifested after the third catalytic reaction, based on inconsistencies between the obtained diffractogram and the one recorded for ZIF-8 and  $\text{PMo}_{12}$ @ZIF-8 without catalytic use (Figure 6c). These structural changes may explain the distinct catalytic behavior observed for  $\text{PMo}_{12}$ @ZIF-8 and  $\text{PMo}_{12}$ @ZIF-67 composites, since immobilized  $\text{PMo}_{12}$  was expected to be comparably accessible for catalysis in both structures. To further investigate the stability of the active center  $\text{Pmo}_{12}$ , an analysis of the  $^{31}\text{P}$  MAS NMR spectroscopy of  $\text{PMo}_{12}$ @ZIF-8 and  $\text{PMo}_{12}$ @ZIF-8-AC

was further performed (Figure 6d). For  $\text{PMo}_{12}@ZIF-8$ ,  $\text{PMo}_{12}$  is mainly expressed by a sharp peak registered at  $-1.8$  ppm, which may represent the isolated  $\text{PMo}_{12}$  incorporated into the MOF framework [46], and a slightly broad protuberance can also be observed at a higher chemical shift (around 7 ppm). This may be attributed to the interaction between  $\text{PMo}_{12}$  and the ZIF-8 framework [22]. The analysis of the catalyst after catalytic use ( $\text{PMo}_{12}@ZIF-8\text{-AC}$ ) presents the same sharp peak; however, the broad peak is now clearly observed around 7.4 ppm. This may indicate a higher interaction of the active center  $\text{PMo}_{12}$  with the ZIF-8 framework promoted by the oxidative catalytic reaction, i.e., further variations on the interaction between  $\text{PMo}_{12}$  and its environment linked to the framework's transformation after catalytic use. This interaction may guarantee the superior catalytic activity of  $\text{PMo}_{12}@ZIF-8$  compared to the  $\text{PMo}_{12}@ZIF-67$ , which probably promoted the alteration of ZIF-8 structure in consecutive ECODS cycles without the occurrence of  $\text{PMo}_{12}$  leaching (confirmed by  $^{31}\text{P}$  NMR analysis of the reaction solution medium at the end of catalytic experiments). On the other hand, the ability of the ZIF-67 to decompose  $\text{H}_2\text{O}_2$  is well reported [47]; however, the quantification of  $\text{H}_2\text{O}_2$  after  $\text{PMo}_{12}@ZIF-67$  catalytic use indicates the presence of at least half of the initial amount of the used oxidant. A similar  $\text{H}_2\text{O}_2$  quantification after catalytic use was found for the ECODS system catalyzed by  $\text{PW}_{12}@ZIF-8$ , indicating the absence of  $\text{H}_2\text{O}_2$  consumption, which was probably caused by an absence of reactant diffusion into pore cavities and the non-occurrence of  $\text{PW}_{12}$  interaction. Therefore, the weakness (using  $\text{PW}_{12}@ZIF-8$ ) or absence (using  $\text{PMo}_{12}@ZIF-67$ ) of the catalytic activity of ZIF-based composites must be associated with a lower diffusion of reactants to their cavities, promoted by the higher POM loadings, or due to the absence of an interaction of the active POM with the MOF framework during the oxidative reaction.

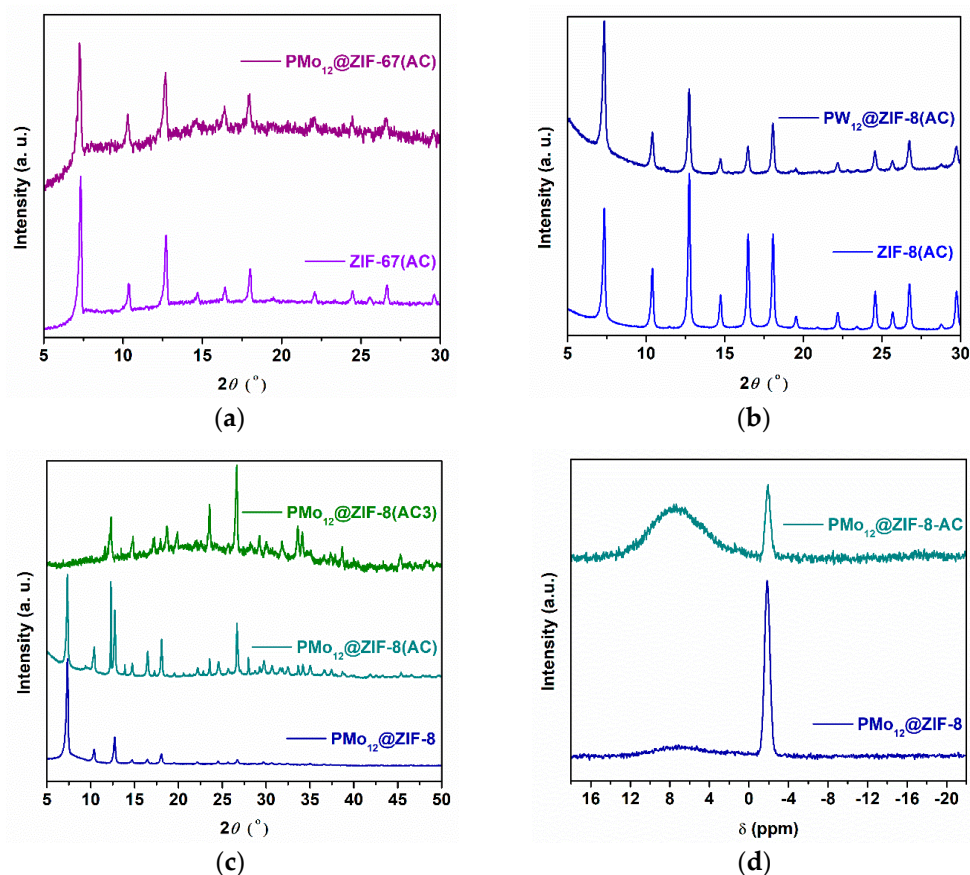


**Figure 6.** Powder XRD patterns obtained for recovered materials after catalysis (AC): (a) ZIF-67(AC) and  $\text{PMo}_{12}@ZIF-67(AC)$ ; (b) ZIF-8(AC) and  $\text{PW}_{12}@ZIF-8(AC)$ ; (c)  $\text{PMo}_{12}@ZIF-8$ ,  $\text{PMo}_{12}@ZIF-8(AC)$  and  $\text{PMo}_{12}@ZIF-8(AC3)$  (AC3 meaning after the 3rd catalytic cycle). (d)  $^{31}\text{P}$  MAS NMR spectra obtained for  $\text{PMo}_{12}@ZIF-8$  and  $\text{PMo}_{12}@ZIF-8\text{-AC}$ .

#### 4. Concluding Remarks

ZIF-based composites encapsulating phosphomolybdic acid ( $\text{PMo}_{12}$ ) and phosphotungstic acid ( $\text{PW}_{12}$ ) were successfully prepared, characterized, and further investigated as heterogeneous catalysts for extraction and catalytic oxidative desulfurization systems (ECODS):  $\text{PMo}_{12}$ @ZIF-8,  $\text{PMo}_{12}$ @ZIF-67, and  $\text{PW}_{12}$ @ZIF-8. The catalytic efficiency of these composites was further compared with the pristine supports ZIF-8 and ZIF-67, and with the homogeneous active centers  $\text{PMo}_{12}$  and  $\text{PW}_{12}$ . The supports revealed an absence of catalytic activity for the desulfurization of a multicomponent model diesel. The  $\text{PMo}_{12}$ @ZIF-8 composite showed a much higher catalytic efficiency to oxidatively desulfurize various benzothiophene derivatives (BT, DBT, MDBT, and DMBDT) than the analogues  $\text{PW}_{12}$ @ZIF-8. The most prominent difference between the composites is in fact their polyoxometalate loading abilities, since the homogeneous catalytic activity of  $\text{PMo}_{12}$  and  $\text{PW}_{12}$  is similar under the studied conditions. The  $\text{PW}_{12}$ @ZIF-8 presents a higher loading (ten times) than the  $\text{PMo}_{12}$ @ZIF-8. This high loading may promote a blockage of ZIF-8 cavities and a low diffusion of reactants, which results in a low catalytic activity of the composite. On the other hand, the  $\text{PMo}_{12}$ @ZIF-67 did not present any catalytic activity, i.e., the incorporation of the highly active  $\text{PMo}_{12}$  into ZIF-67 resulted in an inactive material where the active center  $\text{PMo}_{12}$  cannot fulfill its role as the catalytic active center. In this last composite, a high loading of the guest compounds cannot be the reason for the absence of activity. The nature of the metallic center Co instead of Zn in the ZIF-8 framework, seems to play an important role in the catalytic performance of the catalyst. In fact, an interaction between the  $\text{PMo}_{12}$  and the ZIF-8 supporting structure was found, which is probably the reason for the high catalytic efficiency of the  $\text{PMo}_{12}$ @ZIF-8 composite. This catalyst was recycled for nine consecutive desulfurization cycles, maintaining its activity without the occurrence of  $\text{PMo}_{12}$  leaching.

The work reported in the present manuscript corresponds to a “kick-off” study of this family of composite materials based on Keggin POMs incorporated into porous ZIFs (both ZIF-8 and ZIF-67) to be applied in the desulfurization of model fuels. In fact, the optimization of this type of material composition as well as their thermal modification is now being investigated to improve the catalytic oxidation performance of sulfur-containing compounds.

**Author Contributions:** Conceptualization, S.S.B. and L.C.-S.; methodology, S.S.B., L.C.-S. and M.C.C.; validation, S.S.B. and L.C.-S.; formal analysis, S.S.B. and L.C.-S.; investigation, A.M.V., F.L. and M.C.C.; writing—original draft preparation, A.M.V. and S.S.B.; writing—review and editing, S.S.B. and L.C.-S.; supervision, S.S.B. and L.C.-S.; project administration, S.S.B. and L.C.-S.; funding acquisition L.C.-S. All authors have read and agreed to the published version of the manuscript.

**Funding:** This research work received financial support from Portuguese national funds (FCT/MCTES, Fundação para a Ciência e Tecnologia and Ministério da Ciência, Tecnologia e Ensino Superior) through the strategic project UIDB/50006/2020 (for LAQV-REQUIMTE), LA/P/0037/2020, UIDP/50025/2020, UIDB/50025/2020 (for I3N), and ROTEIRO/0031/2013 – PINFRA/22161/2016 (for PT-NMR). The work also received funding from the European Union (FEDER funds through COMPETE POCI-01-0145-FEDER- 031983).

**Data Availability Statement:** Not applicable.

**Acknowledgments:** L.C.-S., M.C.C. and S.S.B. thank FCT/MCTES for funding through the Individual Call to Scientific Employment Stimulus (Ref. CEECIND/00793/2018, Ref. 2021.03255.CEECIND and Ref. CEECIND/03877/2018, respectively). AMV thanks FCT/MCTES and ESF (European Social Fund) through POCH (Programa Operacional Capital Humano) for his PhD grant (Ref. SFRH/BD/150659/2020).

**Conflicts of Interest:** The authors declare no conflict of interest.

**Sample Availability:** Samples of the compounds can be available by request from the authors.

## References

1. Abas, N.; Kalair, A.; Khan, N. Review of fossil fuels and future energy technologies. *Futures* **2015**, *69*, 31–49. [[CrossRef](#)]
2. Ismagilov, Z.; Yashnik, S.; Kerzhentsev, M.; Parmon, V.; Bourane, A.; Al-Shahrani, F.M.; Hajji, A.A.; Koseoglu, O.R. Oxidative Desulfurization of Hydrocarbon Fuels. *Catal. Rev.* **2011**, *53*, 199–255. [[CrossRef](#)]
3. Samokhvalov, A. Desulfurization of Real and Model Liquid Fuels Using Light: Photocatalysis and Photochemistry. *Catal. Rev.* **2012**, *54*, 281–343. [[CrossRef](#)]
4. Stanislaus, A.; Marafi, A.; Rana, M.S. Recent advances in the science and technology of ultra low sulfur diesel (ULSD) production. *Catal. Today* **2010**, *153*, 1–68. [[CrossRef](#)]
5. Chandra Srivastava, V. An evaluation of desulfurization technologies for sulfur removal from liquid fuels. *RSC Adv.* **2012**, *2*, 759–783. [[CrossRef](#)]
6. Babich, I.V.; Moulijn, J.A. Science and technology of novel processes for deep desulfurization of oil refinery streams: A review. *Fuel* **2003**, *82*, 607–631. [[CrossRef](#)]
7. Campos-Martin, J.M.; Capel-Sanchez, M.C.; Perez-Presas, P.; Fierro, J.L.G. Oxidative processes of desulfurization of liquid fuels. *J. Chem. Technol. Biotechnol.* **2010**, *85*, 879–890. [[CrossRef](#)]
8. Li, J.; Yang, Z.; Li, S.; Jin, Q.; Zhao, J. Review on oxidative desulfurization of fuel by supported heteropolyacid catalysts. *J. Ind. Eng. Chem.* **2020**, *82*, 1–16. [[CrossRef](#)]
9. Long, D.-L.; Tsunashima, R.; Cronin, L. Polyoxometalates: Building Blocks for Functional Nanoscale Systems. *Angew. Chem. Int. Ed.* **2010**, *49*, 1736–1758. [[CrossRef](#)] [[PubMed](#)]
10. Wang, S.-S.; Yang, G.-Y. Recent Advances in Polyoxometalate-Catalyzed Reactions. *Chem. Rev.* **2015**, *115*, 4893–4962. [[CrossRef](#)] [[PubMed](#)]
11. Abazari, R.; Esrafil, L.; Morsali, A.; Wu, Y.; Gao, J. PMo12@UiO-67 nanocomposite as a novel non-leaching catalyst with enhanced performance durability for sulfur removal from liquid fuels with exceptionally diluted oxidant. *Appl. Catal. B Environ.* **2021**, *283*, 119582. [[CrossRef](#)]
12. Du, D.-Y.; Qin, J.-S.; Li, S.-L.; Su, Z.-M.; Lan, Y.-Q. Recent advances in porous polyoxometalate-based metal–organic framework materials. *Chem. Soc. Rev.* **2014**, *43*, 4615–4632. [[CrossRef](#)] [[PubMed](#)]
13. Horcajada, P.; Chalati, T.; Serre, C.; Gillet, B.; Sebrie, C.; Baati, T.; Eubank, J.F.; Heurtaux, D.; Clayette, P.; Kreuz, C.; et al. Porous metal–organic–framework nanoscale carriers as a potential platform for drug delivery and imaging. *Nat. Mater.* **2010**, *9*, 172–178. [[CrossRef](#)]
14. Kreno, L.E.; Leong, K.; Farha, O.K.; Allendorf, M.; Van Duyne, R.P.; Hupp, J.T. Metal–Organic Framework Materials as Chemical Sensors. *Chem. Rev.* **2012**, *112*, 1105–1125. [[CrossRef](#)] [[PubMed](#)]
15. Lee, J.; Farha, O.K.; Roberts, J.; Scheidt, K.A.; Nguyen, S.T.; Hupp, J.T. Metal–organic framework materials as catalysts. *Chem. Soc. Rev.* **2009**, *38*, 1450–1459. [[CrossRef](#)]
16. Li, J.-R.; Kuppler, R.J.; Zhou, H.-C. Selective gas adsorption and separation in metal–organic frameworks. *Chem. Soc. Rev.* **2009**, *38*, 1477–1504. [[CrossRef](#)]
17. Mehtab, T.; Yasin, G.; Arif, M.; Shakeel, M.; Korai, R.M.; Nadeem, M.; Muhammad, N.; Lu, X. Metal-organic frameworks for energy storage devices: Batteries and supercapacitors. *J. Energy Storage* **2019**, *21*, 632–646. [[CrossRef](#)]
18. Viana, A.M.; Juliao, D.; Mirante, F.; Faria, R.G.; de Castro, B.; Balula, S.S.; Cunha-Silva, L. Straightforward activation of metal-organic framework UiO-66 for oxidative desulfurization processes. *Catal. Today* **2021**, *362*, 28–34. [[CrossRef](#)]
19. Granadeiro, C.M.; Barbosa, A.D.S.; Ribeiro, S.; Santos, I.; de Castro, B.; Cunha-Silva, L.; Balula, S.S. Oxidative catalytic versatility of a trivacant polyoxotungstate incorporated into MIL-101(Cr). *Catal. Sci. Technol.* **2014**, *4*, 1416–1425. [[CrossRef](#)]
20. Juliao, D.; Gomes, A.C.; Pillinger, M.; Cunha-Silva, L.; de Castro, B.; Goncalves, I.S.; Balula, S.S. Desulfurization of model diesel by extraction/oxidation using a zinc-substituted polyoxometalate as catalyst under homogeneous and heterogeneous (MIL-101 (Cr) encapsulated) conditions. *Fuel Process. Technol.* **2015**, *131*, 78–86. [[CrossRef](#)]
21. Granadeiro, C.M.; Ferreira, P.M.C.; Juliao, D.; Ribeiro, L.A.; Valenca, R.; Ribeiro, J.C.; Goncalves, I.S.; de Castro, B.; Pillinger, M.; Cunha-Silva, L.; et al. Efficient Oxidative Desulfurization Processes Using Polyoxomolybdate Based Catalysts. *Energies* **2018**, *11*, 1696. [[CrossRef](#)]
22. Mirante, F.; Gomes, N.; Branco, L.C.; Cunha-Silva, L.; Almeida, P.L.; Pillinger, M.; Gago, S.; Granadeiro, C.M.; Balula, S.S. Mesoporous nanosilica-supported polyoxomolybdate as catalysts for sustainable desulfurization. *Microporous Mesoporous Mater.* **2019**, *275*, 163–171. [[CrossRef](#)]
23. Viana, A.M.; Ribeiro, S.O.; de Castro, B.; Balula, S.S.; Cunha-Silva, L. Influence of UiO-66(Zr) Preparation Strategies in Its Catalytic Efficiency for Desulfurization Process. *Materials* **2019**, *12*, 3009. [[CrossRef](#)] [[PubMed](#)]
24. Juliao, D.; Gomes, A.C.; Cunha-Silva, L.; Valenca, R.; Ribeiro, J.C.; Pillinger, M.; de Castro, B.; Goncalves, I.S.; Balula, S.S. A sustainable peroxophosphomolybdate/H<sub>2</sub>O<sub>2</sub> system for the oxidative removal of organosulfur compounds from simulated and real high-sulfur diesels. *Appl. Catal. A-Gen.* **2020**, *589*, 117154. [[CrossRef](#)]
25. Fernandes, S.; Flores, D.; Silva, D.; Santos-Vieira, I.; Mirante, F.; Granadeiro, C.M.; Balula, S.S. Lindqvist@Nanoporous MOF-Based Catalyst for Effective Desulfurization of Fuels. *Nanomaterials* **2022**, *12*, 2887. [[CrossRef](#)]
26. Silva, D.F.; Viana, A.M.; Santos-Vieira, I.; Balula, S.S.; Cunha-Silva, L. Ionic Liquid-Based Polyoxometalate Incorporated at ZIF-8: A Sustainable Catalyst to Combine Desulfurization and Denitrogenation Processes. *Molecules* **2022**, *27*, 1711. [[CrossRef](#)]

27. Saliba, D.; Ammar, M.; Rammal, M.; Al-Ghoul, M.; Hmadeh, M. Crystal Growth of ZIF-8, ZIF-67, and Their Mixed-Metal Derivatives. *J. Am. Chem. Soc.* **2018**, *140*, 1812–1823. [[CrossRef](#)]
28. Mukhopadhyay, S.; Debgupta, J.; Singh, C.; Kar, A.; Das, S.K. A Keggin Polyoxometalate Shows Water Oxidation Activity at Neutral pH: POM@ZIF-8, an Efficient and Robust Electrocatalyst. *Angew. Chem. Int. Ed.* **2018**, *57*, 1918–1923. [[CrossRef](#)]
29. Ghahramaninezhad, M.; Pakdel, F.; Shahrak, M.N. Boosting oxidative desulfurization of model fuel by POM-grafting ZIF-8 as a novel and efficient catalyst. *Polyhedron* **2019**, *170*, 364–372. [[CrossRef](#)]
30. Wang, X.S.; Li, L.; Liang, J.; Huang, Y.B.; Cao, R. Boosting Oxidative Desulfurization of Model and Real Gasoline over Phosphotungstic Acid Encapsulated in Metal-Organic Frameworks: The Window Size Matters. *Chemcatchem* **2017**, *9*, 971–979. [[CrossRef](#)]
31. Lee, Y.-R.; Jang, M.-S.; Cho, H.-Y.; Kwon, H.-J.; Kim, S.; Ahn, W.-S. ZIF-8: A comparison of synthesis methods. *Chem. Eng. J.* **2015**, *271*, 276–280. [[CrossRef](#)]
32. Zhang, L.; Mi, T.; Ziaee, M.A.; Liang, L.; Wang, R. Hollow POM@MOF hybrid-derived porous Co<sub>3</sub>O<sub>4</sub>/CoMoO<sub>4</sub> nanocages for enhanced electrocatalytic water oxidation. *J. Mater. Chem. A* **2018**, *6*, 1639–1647. [[CrossRef](#)]
33. Dai, J.; Li, C.; Xiao, S.; Liu, J.; He, J.; Li, J.; Wang, L.; Lei, J. Fabrication of novel ZIF-67 Composite Microspheres for Effective Adsorption and Solid-phase Extraction of Dyes from Water. *ChemistrySelect* **2018**, *3*, 5833–5842. [[CrossRef](#)]
34. Adnan, M.; Li, K.; Xu, L.; Yan, Y. X-Shaped ZIF-8 for Immobilization Rhizomucor miehei Lipase via Encapsulation and Its Application toward Biodiesel Production. *Catalysts* **2018**, *8*, 96. [[CrossRef](#)]
35. Rocchiccioli-Deltcheff, C.; Aouissi, A.; Bettahar, M.M.; Launay, S.; Fournier, M. Catalysis by 12-Molybdophosphates: 1. Catalytic Reactivity of 12-Molybdophosphoric Acid Related to Its Thermal Behavior Investigated through IR, Raman, Polarographic, and X-ray Diffraction Studies: A Comparison with 12-Molybdosilicic Acid. *J. Catal.* **1996**, *164*, 16–27. [[CrossRef](#)]
36. Zhou, K.; Mousavi, B.; Luo, Z.; Phatanasri, S.; Chaemchuen, S.; Verpoort, F. Characterization and properties of Zn/Co zeolitic imidazolate frameworks vs. ZIF-8 and ZIF-67. *J. Mater. Chem. A* **2017**, *5*, 952–957. [[CrossRef](#)]
37. Wang, L.; Feng, X.; Ren, L.; Piao, Q.; Zhong, J.; Wang, Y.; Li, H.; Chen, Y.; Wang, B. Flexible Solid-State Supercapacitor Based on a Metal-Organic Framework Interwoven by Electrochemically-Deposited PANI. *J. Am. Chem. Soc.* **2015**, *137*, 4920–4923. [[CrossRef](#)]
38. Chang, X.; Yang, X.F.; Qiao, Y.; Wang, S.; Zhang, M.H.; Xu, J.; Wang, D.H.; Bu, X.H. Confined Heteropoly Blues in Defected Zr-MOF (Bottle Around Ship) for High-Efficiency Oxidative Desulfurization. *Small* **2020**, *16*, 1906432. [[CrossRef](#)]
39. Wang, C.; Li, A.R.; Ma, Y.L. Phosphomolybdic acid niched in the metal-organic framework UiO-66 with defects: An efficient and stable catalyst for oxidative desulfurization. *Fuel Process. Technol.* **2021**, *212*, 106629. [[CrossRef](#)]
40. Jafarinasab, M.; Akbari, A. Co-ZIF-67 encapsulated phosphomolybdic acid as a hybrid catalyst for deep oxidative desulfurization. *J. Environ. Chem. Eng.* **2021**, *9*, 106472. [[CrossRef](#)]
41. Wang, C.; Li, A.R.; Ma, Y.L.; Qing, S.L. Preparation of formate-free PMA@MOF-808 catalysts for deep oxidative desulfurization of model fuels. *Environ. Sci. Pollut. Res.* **2022**, *29*, 39427–39440. [[CrossRef](#)] [[PubMed](#)]
42. Yang, N.; Lu, L.J.; Zhu, L.H.; Wu, P.W.; Tao, D.J.; Li, X.W.; Gong, J.H.; Chen, L.L.; Chao, Y.H.; Zhu, W.S. Phosphomolybdic acid encapsulated in ZIF-8-based porous ionic liquids for reactive extraction desulfurization of fuels. *Inorg. Chem. Front.* **2022**, *9*, 165–178. [[CrossRef](#)]
43. Ji, H.F.; Liu, S.T.; Shi, H.F.; Wang, W.D. Phosphomolybdic acid-based sulfur-containing metal-organic framework as an efficient catalyst for dibenzothiophene oxidative desulfurization. *J. Sulfur Chem.* **2022**, *43*, 314–326. [[CrossRef](#)]
44. Zhou, S.S.; He, J.; Wu, P.W.; He, L.W.; Tao, D.J.; Lu, L.J.; Yu, Z.D.; Zhu, L.H.; Chao, Y.H.; Zhu, W.S. Metal-organic framework encapsulated high-loaded phosphomolybdic acid: A highly stable catalyst for oxidative desulfurization of 4,6-dimethyldibenzothiophene. *Fuel* **2022**, *309*, 122143. [[CrossRef](#)]
45. Fernandes, S.C.; Viana, A.M.; de Castro, B.; Cunha-Silva, L.; Balula, S.S. Synergistic combination of the nanoporous system of MOF-808 with a polyoxomolybdate to design an effective catalyst: Simultaneous oxidative desulfurization and denitrogenation processes. *Sustain. Energy Fuels* **2021**, *5*, 4032–4040. [[CrossRef](#)]
46. Mirante, F.; Gomes, N.; Corvo, M.C.; Gago, S.; Balula, S.S. Polyoxomolybdate based ionic-liquids as active catalysts for oxidative desulfurization of simulated diesel. *Polyhedron* **2019**, *170*, 762–770. [[CrossRef](#)]
47. Chen, W.; Chen, F.; Zhang, G.; Kong, S.; Cai, W.; Wang, J.; Du, L.; Wu, C. Fast decomposition of hydrogen peroxide by Zeolitic imidazolate framework-67 crystals. *Mater. Lett.* **2019**, *239*, 94–97. [[CrossRef](#)]

**Disclaimer/Publisher's Note:** The statements, opinions and data contained in all publications are solely those of the individual author(s) and contributor(s) and not of MDPI and/or the editor(s). MDPI and/or the editor(s) disclaim responsibility for any injury to people or property resulting from any ideas, methods, instructions or products referred to in the content.